Published in: Polymer (1999), vol. 40, iss. 10, pp. 2511-2520
Status: Postprint (Author's version)

Composition effect on the core–shell morphology and mechanical properties of ternary polystyrene/styrene–butadiene rubber/polyethylene blends

I. Luzinov, K. Xi, C. Pagnoulle, G. Huynh-Ba and R. Jérôme

Center for Education and Research on Macromolecules (CERM), University of Liège, Institute of Chemistry, B6, Sart-Tilman, 4000 Liège, Belgium

Abstract

The morphology of ternary polystyrene/styrene–butadiene rubber/polyethylene (PS/SBR/PE) blends has been investigated in the limits of a constant content of the major component (PS; 75 wt%) while changing the weight ratio of the two minor constitutive polymers. A core–shell structure for the dispersed phase has been predicted from the spreading coefficients and observed by transmission electron microscopy. Actually, upon increasing the relative content of PE with respect to SBR, the structure of the dispersed phase changes from a multicore structure to a PE/SBR core–shell morphology. The size of the PE subphase in the mixed dispersed phase increases sharply at a PE content that corresponds to phase inversion in the parent SBR/PE binary blends. The ultimate mechanical properties of these blends are sensitive to the strength of the SBR interphase between PS and PE. Some synergism has been observed in the PE/SBR composition dependence of the tensile strengths at yield and break.

Keywords: Polymer blend; Phase morphology; Core–shell morphology

1. Introduction

Multicomponent polymer blends, which consist of at least three or more immiscible polymers, are a new emerging area in the field of polymeric materials. A larger range of phase morphology then becomes available and directly influences the whole set of properties [1-5]. For systems containing two minor phases dispersed in a continuous matrix, three distinct types of phase morphology have to be considered. The first situation corresponds to the independent dispersion of the two minor components. The second extreme situation is where one minor component forms a shell around small domains of the second one. The third situation is the intermediate case, where mixed phases of the two minor components are formed without any ordered organization. The present work will focus on three-component blends in which two minor components are dispersed in the major one, such as to form mixed dispersed phases. In this respect, the tendency for one phase to encapsulate a second one can be predicted by the following equation, which is an alternative form of Harkin's equation [1]:

$$\lambda_{31}=\gamma_{12}-\gamma_{32}-\gamma_{13}, \quad (1)$$

Published in: Polymer (1999), vol. 40, iss. 10, pp. 2511-2520
Status: Postprint (Author's version)

where γ_{12}, γ_{32} and γ_{13} are the interfacial tensions for each component pair, and λ_{31} is defined as the spreading coefficient for the shell forming component 3 on the core forming component 1. The index 2 refers to the matrix. λ_{31} must be positive for component 1 to be encapsulated by component 3.

The objective of this paper is to examine the blend morphology, which can result from the mixing of three immiscible non-reactive polymers, in such a way that the content of the continuous phase forming polymer is constant, whereas the weight ratio of the two minor constitutive components is changed extensively. Attention will also be paid to the relationships between the phase morphology and the ultimate mechanical properties of the blends. In this study, the continuous phase will be a thermoplastic (polystyrene, PS), while a rubber (styrene–butadiene rubber, SBR) and a thermoplastic (polyethylene, PE) will be combined in the dispersed phase. Furthermore, SBRs of two different compositions, and thus of different surface energy and viscosity, will be used in order to find the extent to which these parameters can influence the polyblend properties, and particularly the morphology of the mixed dispersed phase.

Until now, only a few studies have focused on multicomponent (ternary and more) polymer blends. Hobbs et al. [1] investigated three- and four-component polymer blends, and showed that the morphology was consistent with the calculated spreading coefficients for each polymer system. A core–shell morphology was actually reported for the two studied compositions. Nemirovski et al. [2] studied ternary blends consisting of immiscible thermoplastic and thermotropic polymers. The phase morphology was found to be controlled not only by thermodynamic but also by kinetic effects. Finally, mechanical properties were reported for blends in which the core–shell morphology of the dispersed phase resulted from a chemical reaction [3-5]. This phase morphology was shown to affect mechanical properties such as impact strength and modulus.

2. Experimental

2.1. Materials

All the blends investigated in this study contained 75 wt% PS (Polystyrol 158K from BASF), while the two minor components, i.e. a rubber (SBR) and a low-density polyethylene (PE, Shell 33) were used in various mixing ratios. SBR-1 (Shell, Cariflex S1502) and SBR-2 (Shell, Cariflex S1013) contained 23 wt% and 42.7 wt% bound styrene, respectively. Representative properties of these constitutive polymers are listed in Table 1.

Table 1. Main characteristics of the polymers used

Polymer	$M_w \times 10^{-3}$	M_w/M_n	Density (g/cm³)		Torque at 200°C, 10 min mixing (N min)	Elongation[a] (%), ASTM D412	Modulus[a] (MPa), ASTM D4
			20°C	200°C			
PS	250	2.5	1.05[a]	0.97[c]	13	—	—
PE	240[a]	6[a]	0.92[a]	0.75[c]	16	—	—
SBR-1	630	3.5	0.91[b]	0.81[b]	26	630	11.4
SBR-2	418	6.5	0.94[b]	0.84[b]	13	440	17.1

[a] From suppliers.
[b] Calculated by the additive approximation. Data for polybutadiene at 20°C are from Ref. [9]. They have been calculated from Ref. [9] at 200°C.
[c] Ref. [23].

2.2. Blend preparation

Blends were prepared within a Brabender internal mixer under dry nitrogen at 200°C. The constitutive polymers were firstly dry-blended and then melted at 200°C for 2 min in a Brabender chamber at 20 r.p.m. and finally mixed for 10 min at 60 r.p.m. (one-step mixing). In order to avoid oxidation of the components, 0.4 wt% antioxidant (Irganox 1010, Ciba Geigy) was used. The volume of the mixing chamber was 50 ml.

2.3. Transmission electron microscopy and image analysis

Phase morphology was observed with a Philips CM 100 transmission electron microscope. A Reichert–Jung Ultracut FC 4 microtome cooled at −100°C and equipped with a diamond knife was used to prepare the ultrathin sections (70–90 nm thick) from the molded plates prepared for the mechanical testing. These sections were stained by vapor of osmium tetroxide (30 min) and ruthenium tetroxide (2 h), respectively. From the analysis of binary PS/PE and PS/SBR blends stained by this technique, PS was observed as a dark gray phase, SBR as a black one, and the PE phase was light gray. In some cases, only the SBR phase was stained by osmium tetroxide.

The average number of PE particles encapsulated in one SBR domain was calculated as the ratio K, between the number of PE droplets and the number of rubbery domains in which they are dispersed.

Sizes of the PE droplets and the SBR dispersed phases were analyzed by using KS-100 (Kontron Imaging System) software. The apparent number-average diameter (d_n) of these particulate phases was calculated from the analysis of several areas of the sample and more than 150 particles per scanned area. Because of the non-spherical shape of the dispersed phases, the apparent diameters were not converted into absolute values [6]. The phase morphology formed by the two minor components was either a typical core–shell morphology or distinct particles of one component dispersed in a larger (and thus continuous) phase of the second component ('multicore–shell' morphology). The following equation allows one to calculate a, i.e. the shell thickness in the case of core–shell morphology or the average thickness of the 'continuous phase' that separates the near-neighbor discrete particles of the 'multicore' morphology:

$$a = \sqrt{\frac{S_1}{\pi}} - \sqrt{\frac{S_{\text{core}}}{\pi}} = \sqrt{\frac{S_{\text{rub}}}{\pi K}} - \sqrt{\frac{S_{\text{core}}}{\pi}} = 0.5(d_n(\text{rub})/K^{0.5} - d_n(\text{core})), \quad (2)$$

where S_{rub}, S_{core} and S_1 are number-average surface area of the PE-containing SBR phase, the PE core and the SBR phase reduced to one PE particle, respectively, d_n(rub) and d_n(core) are the number-average diameters of the PE-containing SBR phase and the PE core, and K is the average number of PE particles per SBR phase.

2.4. Fracture toughness test

The strength of PS/SBR/PE three-layer assemblies was measured by the asymmetric double cantilever beam test [7]. Plates of PS (1.2 mm thick) and PE (2.2 mm thick) were compression molded at 200°C. A thin film of SBR was spin-coated on PE plates from a toluene solution of different concentrations and the plates were dried overnight at room temperature and then 3 h under vacuum at the same temperature. The PS/SBR/PE sandwich was then assembled and annealed at 200°C for 2 h under low pressure. The thickness of the SBR layers was approximated from the thickness measured by optical interferometery for SBR films spin-coated on glass wafers under the same spinning conditions as those used for the rubber deposition on the PE plates. The fracture test was carried out by inserting a razor blade between the PS and PE plates, and the length of the crack propagating ahead of the razor blade was measured with a traveling microscope after at least 24 h of equilibration at room temperature. The interfacial fracture energy was then calculated as reported elsewhere [7].

2.5. Dynamic mechanical analysis

The shear storage modulus of the blends was measured with a DuPont DMA (model 983) at frequency of 1 Hz and 25°C. Each value is the average of three independent measurements.

2.6. Mechanical properties

Tensile and impact test specimens were machined from molded sheets. The sheets were compression molded at 200°C and 20 MPa for 5 min, and quenched under low pressure.

Stress–strain curves were recorded at room temperature with an Instron tester (model DY24) at a tensile speed of 20 mm/min. The specimens were prepared according to the DIN 53488 standard. The Charpy impact strength was measured at room temperature with a CEAST Fractoscope using notched specimens DIN 53453 (0.3 mm notch). Each tensile or impact value is the average of four to eight independent measurements.

3. Results and discussion

3.1. Morphology

3.1.1. Interfacial tensions and spreading coefficients

In order to correlate the phase morphology and the interfacial tension between the constitutive components, the values of γ_{12}, γ_{32} and γ_{13} have been estimated by using the harmonic mean equation [8] at the mixing temperature (200°C):

$$\gamma_{12} = \gamma_1 + \gamma_2 \frac{4\gamma_1^d \gamma_2^d}{\gamma_1^d + \gamma_2^d} - \frac{4\gamma_1^p \gamma_2^p}{\gamma_1^p + \gamma_2^p}, \quad (3)$$

where the superscripts d and p refer to the dispersive and polar contributions to the surface tension γ, respectively. The spreading coefficients have also been calculated using Eq. (1) from the interfacial tension data. PE, PS and SBR are components 1, 2 and 3, respectively.

Data of surface tension, polarities (γ^p/γ) and change in surface tensions with temperature ($d\gamma/dT$) required for the calculation of the interfacial tensions and spreading coefficients are listed in Table 2. All these data are available in the scientific literature for PE and PS [9-10], while in the case of SBR, they have been supposed to vary linearly with the mole fraction of the constitutive styrene and butadiene components [1]. The surface tension of polybutadiene (PB) has been calculated from parachor data [9]. The polarity of PB is assumed to be the same as for polyisoprene, a methyl derivative of PB. This polarity has been calculated using [10]:

$$\gamma^p/\gamma = (\delta^p/\delta)^2, \quad (4)$$

where δ and δ^p are the polyisoprene solubility parameter and its polar component, respectively [9]. No $d\gamma/dT$ value for PB or polyisoprene is available. Since this property lies in a relatively narrow range (0.056–0.077) for most polymers [9], the surface tension of SBR has been calculated by using two values for $d\gamma/dT$ of PB, i.e. 0.06 and 0.07. Values for γ, γ^p and γ^d at 200°C have been calculated as reported in Table 2. It is worth noting that the polarity is independent of temperature [1]. The interfacial tensions and spreading coefficients were calculated from the surface tension data at 200°C (Table 3). There is no dramatic difference in the values calculated when two distinct values of $d\gamma/dT$ are used for PB (0.06 and 0.07). For the two SBR samples used in this study, the spreading coefficient for the PE/SBR pair is positive, indicating that PE particles must be engulfed in SBR. The interfacial tension between PS and SBR-1 is higher than between PS and SBR-2, whereas the reverse situation is observed for the PE/SBR pairs. All these interfacial tensions are smaller compared to the PE/PS counterpart.

Table 2. Estimated surface tension of polymers at the mixing temperature (200°C)

Polymer	γ (20°C) (mN/m)	Polarity	$-d\gamma/dT$ (mN/m°C)	γ calculated at 200°C (mN/m)		
				γ	γ^d	γ^p
PS	40.7	0.168	0.072	27.8	23.1	4.7
PE	33.7	0	0.06	23	23	0
PB	32	0.03	0.06	21.2	20.6	0.6
PB	32	0.03	0.07	19.4	18.8	0.6
SBR-1[a]				22.1	20.9	1.2
SBR-1[b]				20.5	19.4	1.1
SBR-2[a]				23.1	21.3	1.8
SBR-2[b]				21.7	20.0	1.7

[b] With $-d\gamma/dT$ for PB= 0.06 and 0.07, respectively.

Table 3. Estimated interfacial tensions and spreading coefficients at 200°C

Blend[c]	γ_{13} (mN/m)	γ_{32} (mN/m)	γ_{12} (mN/m)	λ_{31} (mN/m)
PS/SBR-1/PE[a]	1.3	2.2	4.7	1.1
PS/SBR-1/PE[b]	1.4	2.5	4.7	0.8
PS/SBR-2/PE[a]	1.8	1.3	4.7	1.5
PS/SBR-2/PE[b]	1.9	1.6	4.7	1.2

[a] See Table 2.
[c] In this table, PE= 1, PS= 2 and SBR= 3.

3.1.2. Melt viscosity ratios

The phase morphology of polyblends is controlled not only by the interfacial tensions, but also by the melt viscosity or torque ratio [11-13]. Favis and Chalifoux [12] have reported on a well-defined dependence of the phase size on the torque ratio for binary polymer blends. Upon decreasing the torque ratio of the minor phase with respect to the major one down to ca. 0.25, the average particle size of the dispersed phase decreases. Below this ratio, the particle size does not change further, at least in the investigated range. In the particular case of ternary blends with a core–shell structure for the dispersed phase, it might be assumed that the size of the core is influenced by the viscosity ratio of the core forming polymer with respect to the shell precursor. The viscosity ratio between the matrix and the shell phase would then act on the size of the dispersed phase as a whole. From the comparison of the torque ratio (Table 4) for the two PE/SBR and PS/SBR pairs, PE is expected to form smaller subphases in SBR-1 than in SBR-2, whereas SBR-1 would form larger dispersed phases in PS compared to SBR-2. From these predictions based on the torque ratios, it results that thicker rubbery shells around PE are expected to be formed in the case of SBR-1 rather than SBR-2. These qualitative conclusions are in agreement with predictions based on the interfacial tensions. Therefore, the characteristic sizes of the core–shell morphology for PS/SBR/PE ternary systems should change upon substitution of SBR-2 for SBR-1.

Table 4. Values of torque ratio and blend composition at the phase inversion

Polymer pair	Torque ratio at 200°C	PE wt% at the phase inversion
PE/SBR-1	0.62	36
PE/SBR-2	1.2	51
SBR-1/PS	2	—
SBR-2/PS	1	—
PE/PS	1.2	—

From the torque values for the SBR/PE pair, the composition at which the phase inversion occurs in these binary blends can be predicted using [14]:

$$T_1/T_2=\Phi_1/\Phi_2, \quad (5)$$

where T_1 and T_2 are the torque for polymers 1 and 2, and Φ_1 and Φ_2 the volume fraction for each of them. As reported in Table 4, the phase inversion in the SBR/PE binary blends is expected to occur at a lower PE content, when SBR-1 is used rather than SBR-2.

3.1.3. Transmission electron microscopy observations

Fig. 1 illustrates how the phase morphology of the mixed SBR-1/PE dispersed phase depends on the PE content. Whatever this content, PE is always encapsulated by SBR-1, in agreement with the spreading coefficient reported in Table 3 for the PS/SBR-1/PE ternary blends. The internal morphology of the dispersed phase changes with the SBR/PE weight ratio. When the SBR-1/PE weight ratio is such that PE is dispersed in the SBR-1 phase for the parent binary blends, more than one PE particle is usually observed in the SBR-1 droplets (Fig. 1a, b). When the PE content is increased beyond the composition of phase inversion, much larger and much more irregularly shaped PE subphases are observed (Fig. 1c), which become regular in shape and closely follow the contour line of the SBR-1 phase at PE contents far beyond the phase inversion (Fig. 1d). In this case, some SBR subinclusions are observed within the PE particles.

The average number of PE subphases per SBR dispersed phase has been calculated by image analysis and reported as the *K* parameter. Fig. 2 shows that *K* decreases from ca. 2.2 to 1.0 when the PE content in SBR-1 is increased.

Published in: Polymer (1999), vol. 40, iss. 10, pp. 2511-2520
Status: Postprint (Author's version)

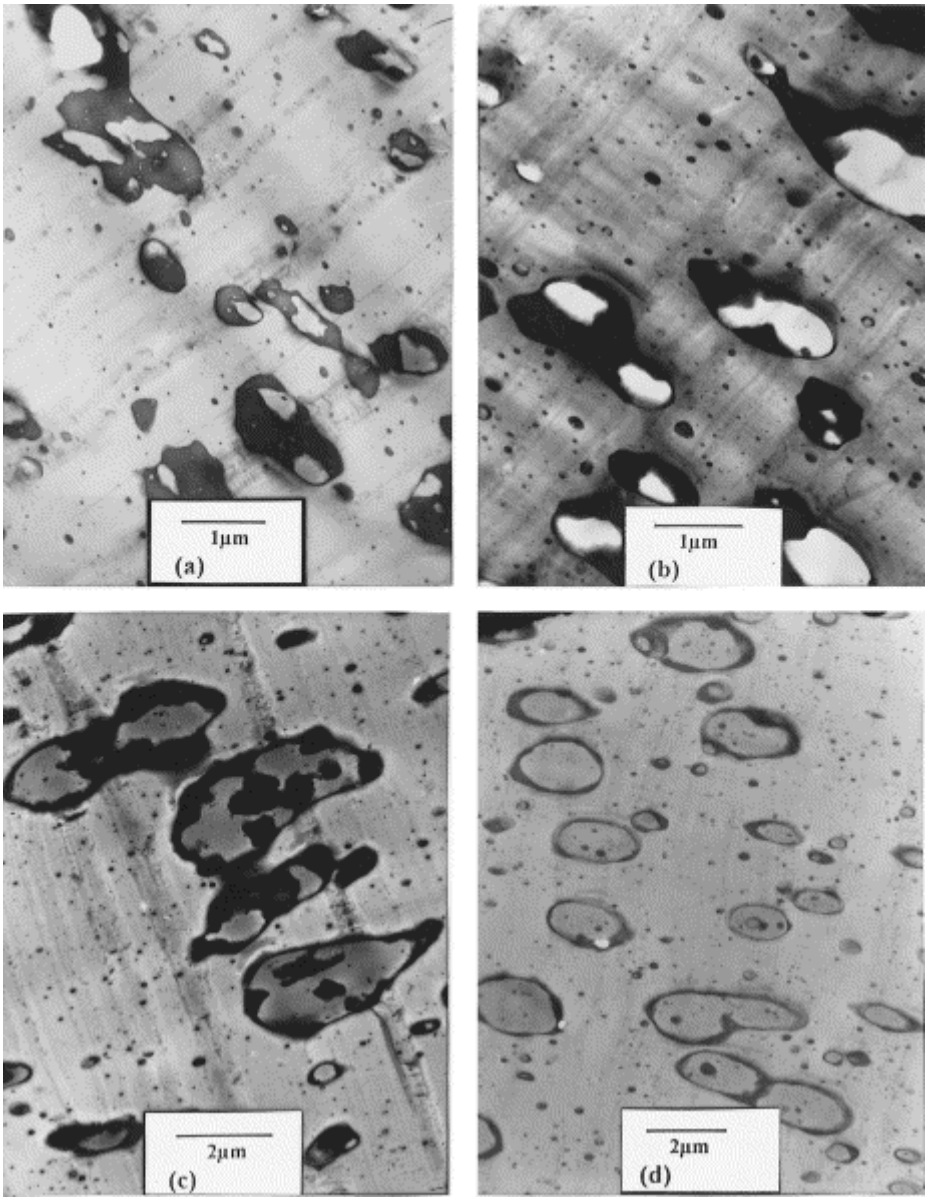

Fig. 1. Transmission electron micrographs of PS/SBR-1/PE blends of different PE contents in the mixed SBR-1/PE dispersed phase: (a) 28%; (b) 38%; (c) 50%; (d) 64%.

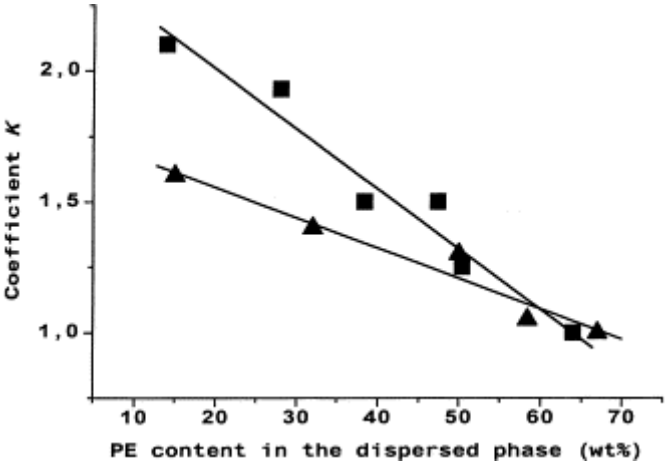

Fig. 2. Effect of the dispersed phase composition on the ratio K, for blends containing SBR-1 (▪) and SBR-2 (▲).

Published in: Polymer (1999), vol. 40, iss. 10, pp. 2511-2520
Status: Postprint (Author's version)

Fig. 3 shows the morphological changes for the PS/SBR-2/PE blends. Similarly to the blends consisting of SBR-1, PE systematically forms subphases in the SBR-2 phase. At low PE contents, more than one PE subphase is usually observed in the SBR-2 domains (Fig. 3a, b). At PE content close to and higher than the theoretical composition of phase inversion for SBR-2/PE, the binary blends, each PE subphase is observed as coated by an SBR-2 shell (Fig. 3c, d). For these blends, there are subinclusions of SBR-2 in the PE phase, particularly for blends with the highest PE content.

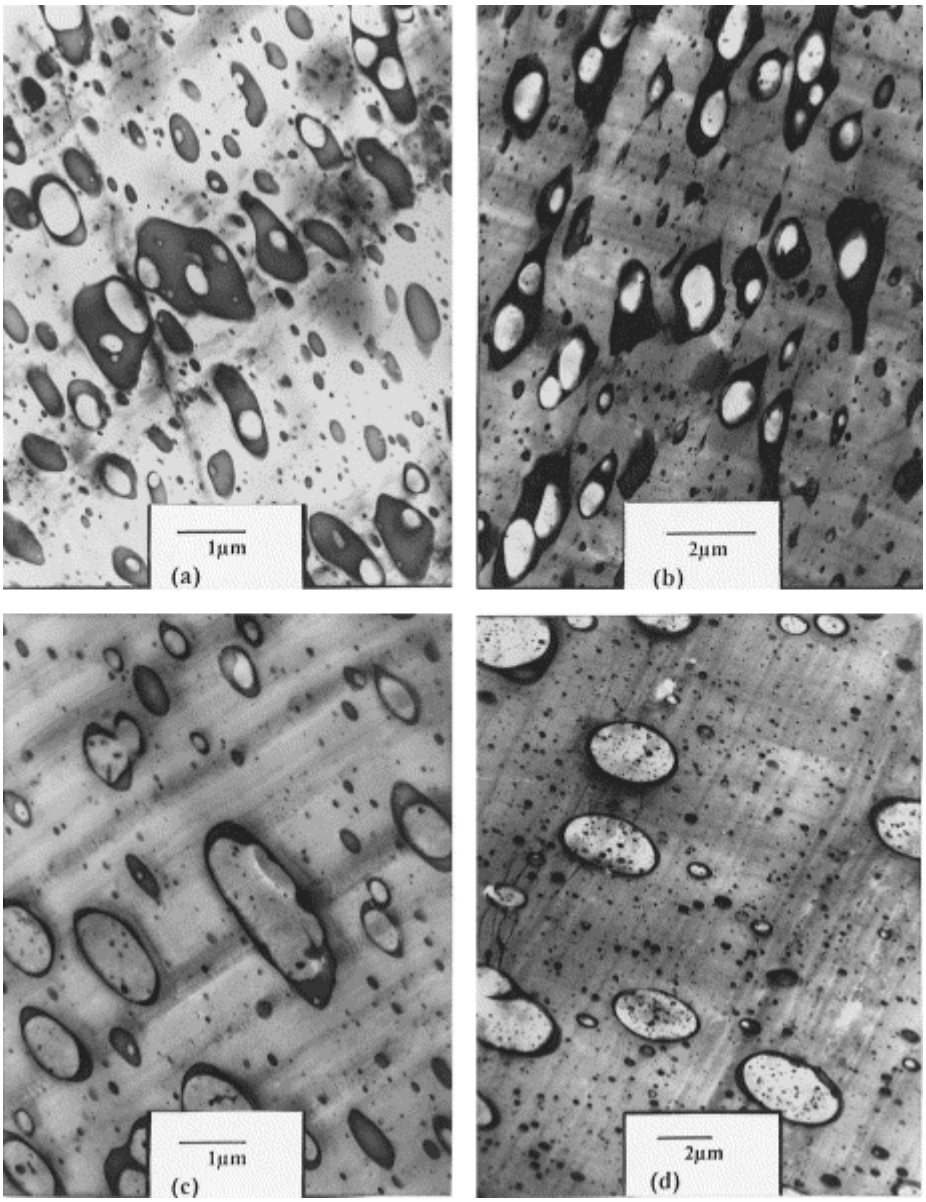

Fig. 3. Transmission electron micrographs of PS/SBR-2/PE blends of different PE contents in the mixed SBR-2/PE dispersed phase: (a) 15%; (b) 32%; (c) 50%; (d) 67%.

Dependence of *K* on the PE content (Fig. 2) confirms these qualitative observations, although the subdivision of PE within SBR-2 is less important than in SBR-1. It must be pointed out that the shape of the dispersed SBR-1 and SBR-2 phases is irregular at low PE content (<50 wt%) and becomes much more regular when PE becomes the major component (Fig. 1 and Fig. 3).

Published in: Polymer (1999), vol. 40, iss. 10, pp. 2511-2520
Status: Postprint (Author's version)

3.1.4. Size of the PE core

The number-average diameter of the PE subphases in the dispersed rubbery phase is plotted versus the dispersed phase composition in Fig. 4. For each series of blends, the particle size increases with the PE content in the dispersed phase. Indeed, the diameter increases from 0.26 to 1.31 μm, and from 0.45 to 1.91 μm for the SBR-1- and SBR-2-containing polyblends, respectively. It is, however, worth noting that the particle size increases very sharply at the composition of phase inversion for the two series of PE/SBR-1 and PE/SBR-2 binary blends. This observation can be explained as follows. In converting to what happens in binary SBR/PE blends, the thermodynamics of the ternary PS/SBR/PE blends prevents PE from being continuous in the mixed SBR/PE dispersed phase when it is the major component. SBR subinclusions in the PE particles are, however, reminiscent of this tendency of PE to envelop SBR at PE contents larger than the theoretical phase inversion. In this composition range, the tendency of PE to coalesce and SBR to form subinclusions explain why there is such a rapid increase in the PE core size.

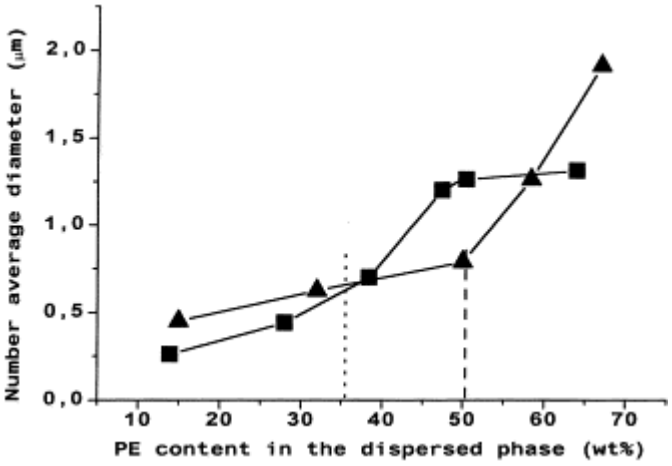

Fig. 4. Effect of the dispersed phase composition on the number-average diameter of the PE particles, for blends containing SBR-1 (▪) and SBR-2 (▲). Dotted and dashed lines indicate the phase inversion composition for SBR-1/PE and SBR-2/PE binary blends, respectively.

From the values of interfacial tension and torque ratio, the PE domains should be larger in blends containing SBR-2 rather than SBR-1. The experimental observations support the validity of these predictions, since much larger PE particles are observed in the case of SBR-2 compared to SBR-1 (except for the phase inversion range). Moreover, at high PE contents, the PE particle size in the presence of SBR-2 tends to increase continuously and not to level off, as observed in the SBR-1 rubbery phase.

3.1.5. Thickness of the SBR shell

Fig. 5a shows how the thickness of the SBR layer around the PE particles changes with the dispersed phase composition. For the SBR-2-containing blends, the thickness steadily decreases with increasing PE content, which is the expected behavior, since less SBR (compared to PE) is available. The situation is more complex in the case of SBR-1, since the thickness increases first with the PE content before decreasing. This observation must be related to the very small size of the PE subphases in SBR-1 at low PE content.

Published in: Polymer (1999), vol. 40, iss. 10, pp. 2511-2520
Status: Postprint (Author's version)

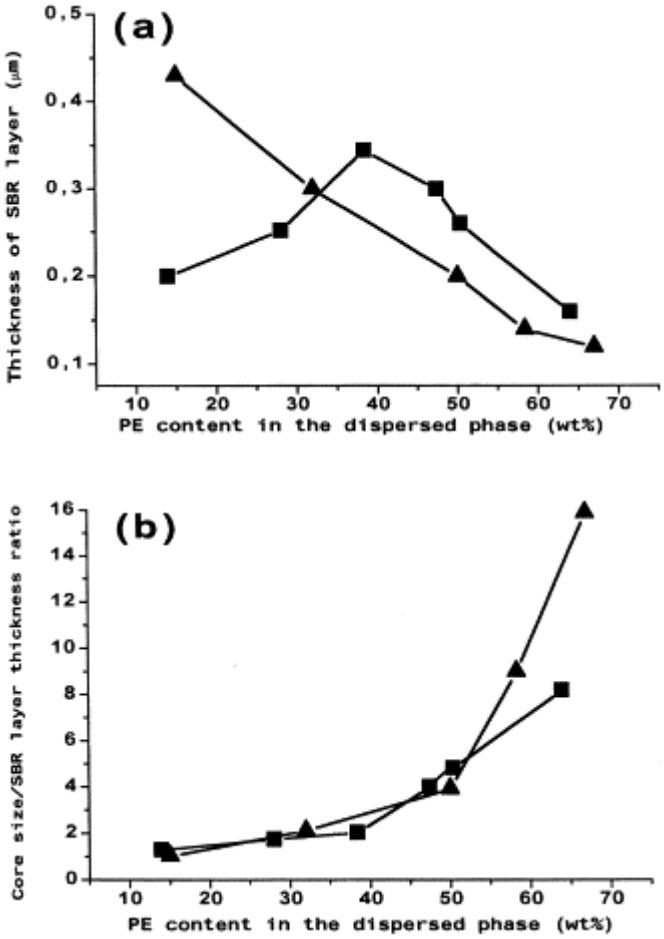

Fig. 5. Effect of the dispersed phase composition on the thickness of the SBR layer (a) and the ratio between the core size and the SBR layer thickness (b), for blends containing SBR-1 (▪) and SBR-2 (▲).

Moreover, from the interfacial tension and torque ratio for the PS/SBR pair, the size of the SBR domains is predicted to be larger for SBR-1 compared to SBR-2, which accounts for the larger thickness of the SBR-1 layers in the dispersed phase that exceed 35 wt% PE. Thus, the dependence of the layer thickness on the composition of the dispersed phase changes with the shell forming polymer, SBR-1 and SBR-2, and thus with the thermodynamic/viscoelastic characteristics of the two polymer pairs PS/SBR and SBR/PE.

It is worth noting that the ratio between the diameter of the PE cores and the thickness of the SBR shells in the dispersed phase is essentially independent of the rubbery phase (SBR-1 or SBR-2) at PE contents up to 55 wt% (Fig. 5b).

3.2. Mechanical properties

3.2.1. Toughness of PS/SBR/PE assemblies

Fig. 6 shows how the interfacial fracture energy (G_c) of these three-layer assemblies depends on the thickness of the central SBR layer. G_c initially increases with the SBR thickness and passes through a maximum for a 100 nm-thick rubber layer whatever the rubber, SBR-1 or SBR-2, and then decreases more rapidly for SBR-1 than for SBR-2. It is noteworthy that G_c of the bare PS/PE interface is systematically improved by the SBR layer in a manner that depends on its thickness. The surfaces of the PE and PS plates have been observed by optical microscopy after testing. When the original thickness of the SBR layer exceeds 0.3 μm, it is clear that the sample failure occurs through the SBR layer. When the SBR layer is thinner, the optical microscopy technique is no longer sensitive enough to ascertain that the PS and PE plates are coated by SBR after separation. From this preliminary observation, it appears that the SBR copolymers are adherent to both PE and PS, possibly as a result of segmental interdiffusion between SBR and PS, on the one hand, and between the rubber and PE on the other.

G_c is definitely larger for SBR-2 beyond the maximum value. This difference would be consistent with the higher ultimate tensile strength of SBR-2, which contains more styrene than SBR-1.

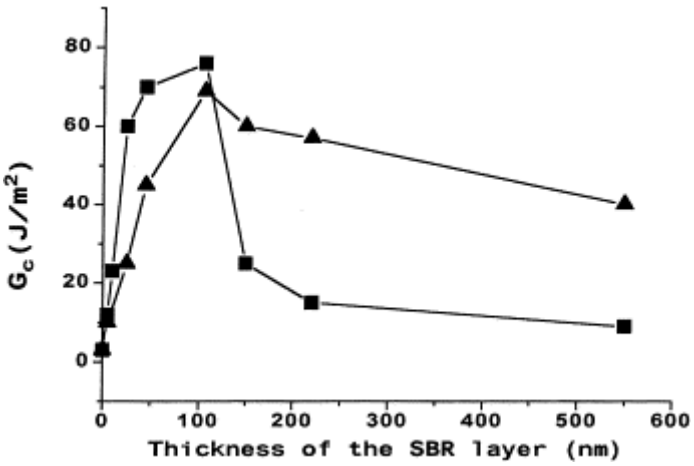

Fig. 6. Fracture toughness of PS/SBR-1/PE (▪) and PS/SBR-2/PE (▲) three-layer assemblies as a function of the rubber layer thickness.

3.2.2. Shear storage modulus

The shear storage modulus of the ternary blends is plotted in Fig. 7 versus the composition of the mixed dispersed phase. This modulus allows the stress transfer from the matrix to the components of the dispersed phase to be estimated under conditions of very low non-destructive deformations, in contrast to what happened in the previous measurements of the interface toughness. These plots are qualitatively comparable for the two types of SBR. At low PE contents in the dispersed phase, the modulus does not change significantly. When this content is close to ca. 50%, a sharp increase in the modulus occurs. Further addition of PE does not change the modulus of the SBR-1-containing blends very much, but decreases the storage modulus of the SBR-2 counterparts, possibly because of the significant amount of SBR-2 subinclusions in the PE core (Fig. 3d).

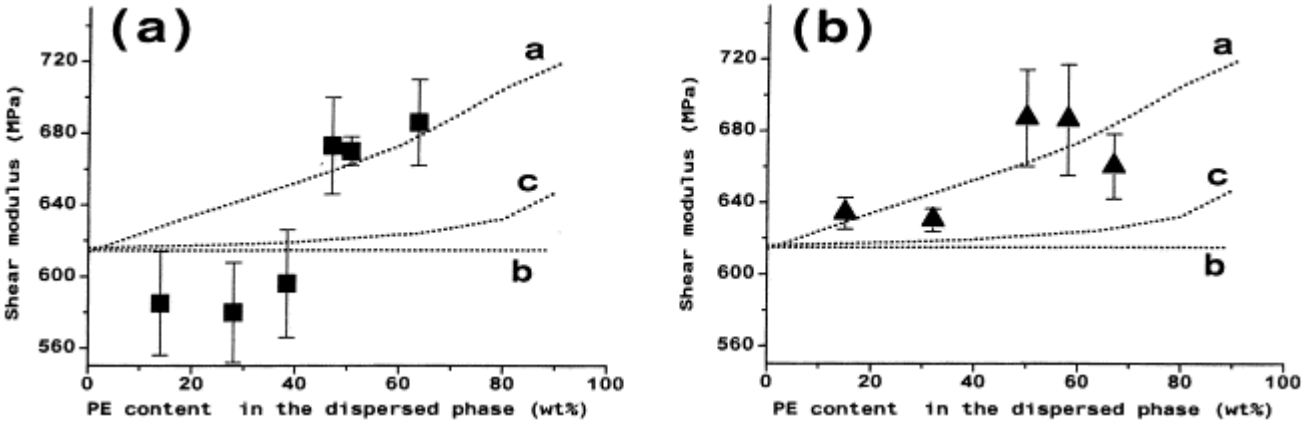

Fig. 7. Shear storage modulus and theoretical predictions based on (6) and (7) in relation to the PE content of the dispersed phase, for blends containing SBR-1 (a) and SBR-2 (b). Lines a, b and c correspond to the upper bound of interfacial situation (1), to the interfacial situations (2), (3) and (4), and to the Rösch model, respectively.

Several theories have been proposed to predict the modulus of two-phase composites [15-18], which have recently been extended to binary [19-20] and ternary [5] polymer blends. In the case of spherical dispersed phases, Kerner [15] derived the following equation:

$$E = E_1 \frac{\frac{\phi_2 E_2}{(7-5\nu_1)E_1+(8-10\nu_1)E_2} + \frac{\phi_1}{15(1-\nu_1)}}{\frac{\phi_2 E_1}{(7-5\nu_1)E_1+(8-10\nu_1)E_2} + \frac{\phi_1}{15(1-\nu_1)}}, \quad (6)$$

where E, E_1 and E_2 are the moduli for the binary blend, the matrix and the dispersed phase, respectively; ϕ_1, ϕ_2 are the volume fractions of the matrix and the dispersed phase, respectively; and ν_1 is the Poisson ratio for the matrix. This equation is valid in the case of an ideal stress transfer through the interface. When no stress is transferred or the matrix is much more rigid than the dispersed phase, the Kerner equation is simplified, since E_2 is then assumed to be zero:

$$E = E_1 \frac{1}{1 + (\phi_2/\phi_1)\,[15(1-\nu_1)/(7-5\nu_1)]}. \quad (7)$$

For the blends under consideration, four distinct interfacial situations may be identified: (1) perfect stress transfer from the PS matrix to the SBR shell and through the shell to the PE core; (2) perfect transfer from PS to SBR, but not through SBR to PE; (3) poor stress transfer from the matrix to the SBR shell and perfect transfer from SBR to PE; (4) poor stress transfer from PS to SBR and from SBR to PE. Cases (2)–(4) are comparable, since no stress transfer may occur from the PS matrix to the PE core. In this extreme situation, the modulus of the PS/SBR/PE ternary blends may be approximated to the modulus of the binary PS/SBR blend with the same PS content (75 wt%) calculated by Eq. (7), because of the very low value of the SBR modulus. Curve b in Fig. 7a and b corresponds to this extreme case. Case (1) is the other extreme situation, since as a result of a strong adhesion at the two interfaces, the stress may be supposed to be transfered from the matrix to the PE phase through SBR. The modulus can then be calculated from the Kerner model by assuming that the stress distribution is uniform in the PS and SBR phases, and that the average stress is actually the macroscopic stress in the PS/SBR binary blend of the same relative content as in the ternary blend. Therefore, the modulus of the binary PS/SBR blends of different compositions has first been calculated by Eq. (7). Eq. (6) has been used to calculate the modulus of ternary blends, while considering the PS/SBR blend as the matrix and PE as the dispersed phase. The Poisson ratio for PS is 0.38, and 0.50 for SBR and PE [9 ; 21]. Since the Kerner model has proved to be largely insensitive to variations in the Poisson ratio [5], this ratio for the PS/SBR 'matrix' has been supposed to be the same as for PS. The shear storage moduli for PS (1040 mPa), PE (210 mPa), SBR-1 (0.5 mPa) and SBR-2 (1 mPa) have been determined by dynamic mechanical measurements. Curve a in Fig. 7a and b has been computed accordingly.

The modulus of ternary blends with a core–shell structure can, however, be approximated in a different way, as proposed by Rösch [5]. In the case of perfect stress transfer between the phases, the stress distribution is supposed to be uniform in the SBR and PE dispersed phases. The modulus of the binary dispersed particles is then calculated using Eq. (6), where SBR is the matrix and PE the dispersed phase. The modulus of the ternary blends is also calculated using Eq. (6), PS now being the matrix and the modulus of the dispersed phase being the value calculated in the first step. Curve c, which results from this calculation by the Rösch method, is shown in Fig. 7a and b.

When SBR-1 is the rubber, curves a and b in Fig. 7a can account for the experimental moduli. At low PE contents, no stress is transferred to the PE core. When SBR-2 is substituted for SBR-1, some transfer occurs in a possible relation to the higher styrene content of SBR-2 compared to SBR-1, resulting in a better PS/SBR adhesion and a higher stiffness of the rubbery layer. At PE contents higher than 40%, the stress transfer from the matrix to the core seems to become ideal, whatever the rubber used. However, at a PE content of ca. 60%, this transfer from PS to PE seems to be less efficient for SBR-2, possibly because of the significant amounts of SBR-2 subinclusions in the PE subphase.

Fig. 8 shows the dependence of the shear storage modulus on the ratio between the core size and the SBR layer thickness in the dispersed phase. When this ratio is small (<0.2), the modulus is essentially constant, although higher for the SBR-2-containing blends than the SBR-1 ones. There is some increase in the modulus when the core size increases with respect to the SBR layer (in the range from 3 to 4), in qualitative agreement with a more efficient stress transfer from the PS matrix to the PE cores. Any further increase in the core size/SBR layer thickness ratio (from 4 to 8) does not change the modulus further.

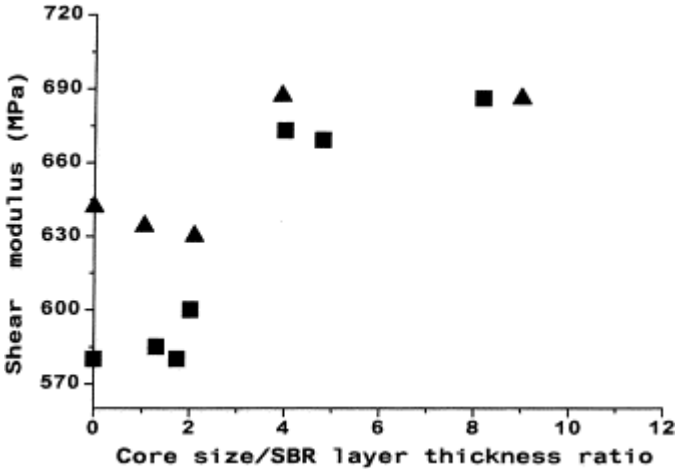

Fig. 8. Shear storage modulus as a function of the core size/SBR layer thickness ratio, for blends containing SBR-1 (▪) and SBR-2 (▲).

3.2.3. Tensile properties and impact strength

Compared to the PS/PE binary blend, which is brittle, the parent PS/SBR/PE blends show higher performances, particularly when SBR-2 is the rubber. The ultimate mechanical properties, including the yield stress of these blends, are shown in Fig. 9, Fig. 10, Fig. 11 and Fig. 12, in relation to the PE content in the dispersed phase. Except for the elongation, the superiority of the SBR-2-containing blends is clear over the SBR-1 counterparts. It is noteworthy that these blends show some positive deviation for the tensile strengths at yield and break from the ideal additive behavior which is usually predicted by the so-called mixing rule [22].

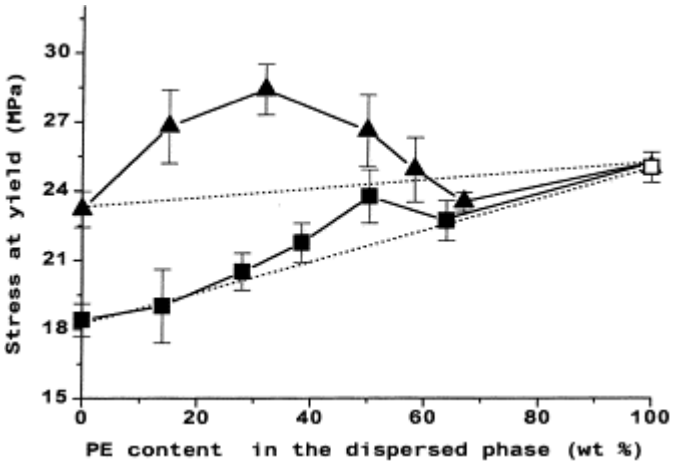

Fig. 9. Tensile stress at yield versus the PE content in the dispersed phase for blends containing SBR-1 (▪) and SBR-2 (▲). Dotted lines are predictions by the mixing rule. Open symbols refer to brittle failure.

Published in: Polymer (1999), vol. 40, iss. 10, pp. 2511-2520
Status: Postprint (Author's version)

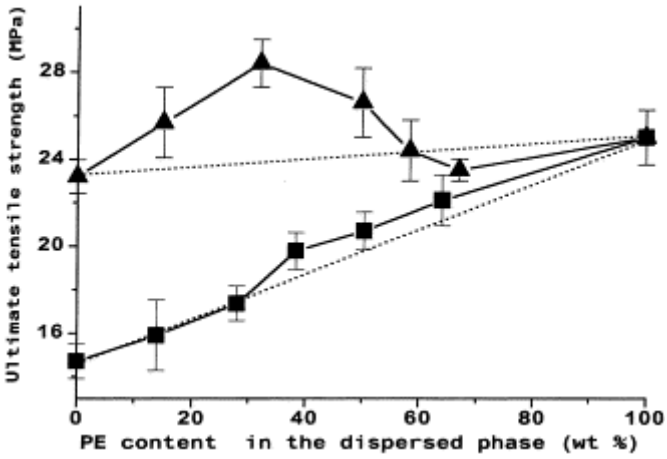

Fig. 10. Ultimate tensile strength versus the PE content in the dispersed phase for blends containing SBR-1 (▪) and SBR-2 (▲). Dotted lines are predictions by the mixing rule.

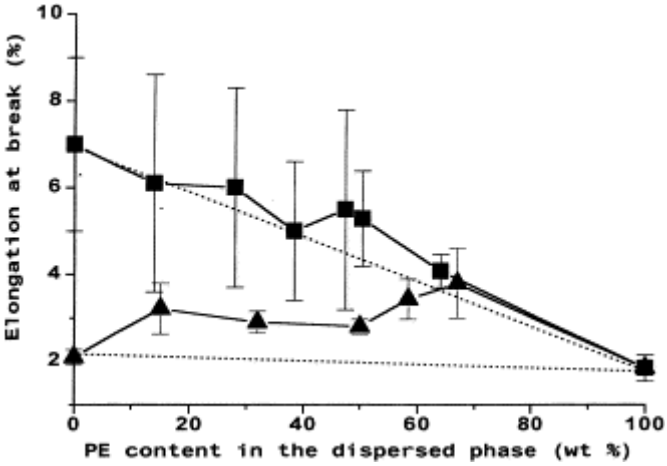

Fig. 11. Elongation at break versus the PE content in the dispersed phase for blends containing SBR-1 (▪) and SBR-2 (▲). Dotted lines are predictions by the mixing rule.

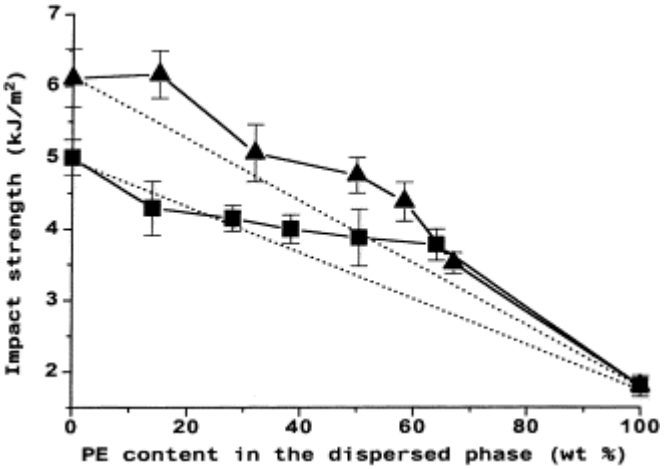

Fig. 12. Impact strength versus the PE content in the dispersed phase for blends containing SBR-1 (▪) and SBR-2 (▲). Dotted lines are predictions by the mixing rule.

A parallel could be drawn between the higher mechanical performances of the SBR-2-containing blends and the higher interfacial strength of the PS/SBR-2/PE three-layer assembly compared to the SBR-1-based systems. This observation might indicate that the SBR shell is deformed during the strain and that the blend failure originates from rupture of the PS/SBR/PE interphase. The stress transfer through the rubbery shell during stress–strain measurements should then be more efficient in the case of SBR-2 compared to SBR-1.

4. Conclusions

The morphology of the ternary PS/SBR/PE blends has been investigated in relation to the weight ratio of the minor components (SBR and PE) that form the dispersed phase in PS. PE systematically forms cores in SBR. The average number of PE cores per SBR phase decreases when the PE content in SBR is increased, and finally only one PE subphase is observed in SBR, that actually forms a shell around a PE core and provides the dispersed phase with a core–shell morphology. The size of the core suddenly increases at the PE content in the mixed dispersed phase that actually corresponds to the composition of the phase inversion in the binary SBR/PE blends. The well-known control of the phase morphology of binary blends by the interfacial tension and the torque ratio of the constitutive components is also observed in ternary blends, although within some limits of blend composition.

Comparison of the experimental shear storage modulus with the Kerner model indicates that perfect stress transfer from the matrix through the shell to the core occurs when the ratio between the size of the core and the thickness of the SBR layer is high enough. There is no negative deviation for the ultimate mechanical properties with respect to the mixing rules for the blends containing dispersed phases of different compositions. Rather, some synergism in tensile strengths at yield and break has been observed for SBR-2-containing ternary blends. The strength of the PS/SBR/PE interphase seems to be of critical importance for the ultimate mechanical properties.

Acknowledgements

We are grateful to the 'Services Fédéraux des Affaires Scientifiques, Techniques et Culturelles' for general support in the frame of the 'PAI-4: Chimie et Catalyse Supramoléculaire'. We also thank Mrs Martine Dejeneffe for transmission electron microscope observations and Mr P.A. Blanche (Centre Spatial de Liège) for optical interferometery measurements. I.L. is indebted to the NATO Science Committee (Belgium) for a fellowship.

References

[1] Hobbs SY, Dekkers MEJ, Wafkins VH. Polymer 1988;29:1598.
[2] Nemirovski N, Siegmann A, Narkis N. J Macromol Sci, Phys 1995;34B:459.
[3] Horiuchi S, Matchariyakul N, Yase K, Kitano T, Choi HK, Lee YM. Polymer 1996;37:3065.
[4] Horiuchi S, Matchariyakul N, Yase K, Kitano T, Choi HK, Lee YM. Polymer 1997;38:59.
[5] Rôsch J. Polym Eng Sci 1995;35:1917.
[6] Oshinski AJ, Keskkula H, Paul DR. Polymer 1996;37:4891.
[7] Cretan C, Kramer EJ, Hui CY, Brown HR. Macromolecules 1992;25:3075.
[8] Wu S. J Polym Sci, Part C 1971;34:19.
[9] van Krevelen DW. Properties of polymers, chaps. 4, 7 and 8. Amsterdam: Elsevier, 1990.
[10] Wu S. In: Brandrup J, Immergut EH, editors. Polymer handbook, chap. 6. New York: Wiley, 1989: 411.
[11] Favis BD. Macromol Chem, Macromol Symp 1992; 56:143.
[12] Favis BD, Chalifoux JP. Polym Eng Sci 1987; 27:1591.
[13] Wu S. Polym Eng Sci 1987; 27:335.
[14] Avgeropoulos GN, Weissert FC, Biddison PH, Bôhm GGA. Rubber Chem Technol 1976;49:93.
[15] Kerner EH. Proc Phys Soc 1956;69B:808.
[16] Hashin Z, Shtrikman S. J Mech Phys Solids 1963; 11:127.
[17] Uemura S, Takayanagi M. J Appl Polym Sci 1966; 10:113.
[18] Kraus G, Rollman KW. Adv Chem Ser 1971;99:189.
[19] Leclair A, Favis BD. Polymer 1996; 37:4723.
[20] Kunory T, Geil PH. J Macromol Sci, Phys 1980;18B:93.
[21] Donatelli AA, Sperling LH, Thomas DA. Macromolecules 1976;9:676.
[22] Kolarik J, Lednicky F, Pukanszky B, Pegoraro M. Polym Eng Sci 1992;32:886.
[23] Mekhilef M, Verhoogt H. Polymer 1996;37:4069.